# Photocatalytic Oxidation of Azo Dyes and Oxalic Acid in Batch Reactors and CSTR: Introduction of Photon Absorption by Dyes to Kinetic Models



**I. Grčić[a,b,*] and N. Koprivanac[a]**

[a]University of Zagreb, Faculty of Chemical Engineering and Technology, Marulićev trg 19, HR-10000 Zagreb, Croatia

[b]University of Zagreb, Faculty of Geotechnical Engineering, Hallerova aleja 7, HR-42000 Varaždin, Croatia

doi: 10.15255/CABEQ.2016.974

Original scientific paper
Received: September 6, 2016
Accepted: February 10, 2018

*In loving memory of our dear friend and colleague Dinko Vujević*

The possibilities of treating industrial effluents and water purification by advanced oxidation processes have been extensively studied; photocatalysis has emerged as a feasible alternative solution. In order to apply the photocatalytic treatment on a larger scale, relevant modeling approaches are necessary. The scope of this work was to investigate the applicability of recently published kinetic models in different reactor systems (batch and CSTR) under UVA or UVC irradiation and in combination with two types of $TiO_2$ catalyst, AEROXIDE® P25 and PC-500 for degradation of azo dyes (C.I. Reactive Violet 2, and C.I. Mordant Yellow 10), oxalic acid and their mixtures. The influences of reactor geometry and irradiation intensities on pollutant oxidation efficiency were examined. The effect of photon absorption by dyes in water matrix was thoroughly studied. Relevant kinetic models were introduced to the mass balance for particular reactor system. Resulting models were sufficient for description of pollutant degradation in batch reactors and CSTR. Experimental results showed 1.15 times higher mineralization extents achieved after 7 cycles in CSTR than in batch photoreactor of similar geometry within the equivalent time-span. The application of CSTR in-series could simplify the photocatalytic water treatment on a larger scale.

*Keywords:*
photocatalysis, colored wastewater, azo dyes, oxalic acid, modeling, kinetics

## Introduction

Wastewater polluted with potentially toxic organic substances presents a serious threat to the environment. The colored wastewaters generated during dye manufacturing and dye application processes represent a specific problem in the achievement of desired water quality. The conventional wastewater treatment technologies are inefficient for complete degradation of organic dyes[1–4]. To overcome those issues, advanced treatment methods have been adopted recently. The advanced oxidation processes (AOPs) have received special attention, due to their capacity for meeting increasingly stringent wastewater standards[5]. All AOPs consider the in-situ generation of very reactive oxidizing species, primarily hydroxyl radicals ($OH^{\bullet}$) for degradation of organic compounds[6]. Generation of $OH^{\bullet}$ radicals can be enhanced by employing various systems, i.e. UV/catalyst, UV/catalyst/$H_2O_2$, $O_3$/$H_2O_2$, UV/$O_3$/$H_2O_2$, UV/$O_3$/catalyst, Fe(II)/Fe(III) with $H_2O_2$ (Fenton reaction), and UV/{Fe(II)/Fe(III)+$H_2O_2$} (photo-Fenton)[7]. Among various alternative wastewater treatment processes, semiconductor photocatalysis is the most studied heterogeneous catalytic process in last decade. Photocatalysis is an attractive oxidation process for a wide range of water- and air-borne organics without harmful environmental impacts[8]. The $TiO_2$ is the most widely used semiconductor photocatalyst for wastewater treatment. Despite numerous attempts for finding a substitute for $TiO_2$, it is still considered an optimal catalyst, since it is non-toxic and resistant to photocorrosion over a wide range of pH and is relatively easy to produce and apply at lower costs[6]. The design of an efficient photocatalytic reactor is an important aspect in improving the efficiency of photocatalytic oxidation process. Proper design requires a comprehensive study of the mathematical models to assist the design equations, scale-up and optimization based on laboratory experiments.

The key step in photocatalysis is the generation of hole-electron ($h^+/e^-$) pairs in the semiconductor ($TiO_2$ particle), which migrate to the surface, whereby

*Corresponding author. Tel.: +385 42 408 945; fax: +385 1 4597 143; E-mail address: ivana.grcic@gfv.hr

the recombination competes with the interfacial charge transfer to the adsorbed species, such as oxygen, water, organic and inorganic substances. The oxidation of organic substances presumably proceeds through distinct routes: (i) via •OH radicals generated upon hole trapping by $OH^-$ or adsorbed water molecules or (ii) by direct hole transfer to an adsorbed pollutant, i.e. photo-Kolbe reaction mechanism, Eq. (1).

$$R\text{-}COO^- + h^+ \rightarrow R\bullet + CO_2 \quad (1)$$

Several studies have confirmed the preferred oxidation mechanism of aromatic substances via •OH-attack, especially in the case of photodegradation of halogenated molecules, while the photodegradation of aliphatic acids normally favors the $h^+$ trapping path[9,10]. Recent studies imply that the overall photodegradation of oxalic acid occurs due to the combination of two pathways working in parallel. In addition, two kinetic regimes were observed by analyzing the photodegradation reaction rate; fast first order and slow half reaction order kinetics were associated with •OH-attack and direct $h^+$ trapping by the adsorbed oxalic acid/oxalate molecules, respectively[11,12].

Moreover, the Langmuir-Hinshelwood (L-H) mechanism was successfully applied to describe the kinetics of photocatalytic reaction of a wide range of organic pollutants over illuminated $TiO_2$ surface[9,12,13]. In the previous work, the authors showed that degradation of pollutant, e.g., dye can be simplified and described as first-order equation[14]. Generally, simplification of L-H kinetic model to the first-order rate equation is appropriate for a concentration below a few ppm; several studies have reported the accurate fit[13,15–17].

This work presents a sequel of our previous studies, whereby $TiO_2$ photocatalysis was applied for destruction of two groups of model pollutants, i.e. aliphatic (oxalic acid) and aromatic (azo dyes). Having in mind the absorption of incident UVA and UVC irradiation by azo group in dye molecule, there is a significant difference in the incident light absorption properties and the complexity of corresponding degradation mechanisms[18,19]. In this study, photocatalytic efficiencies of two different commercially available $TiO_2$ powders; P25 by Evonik and PC500 by Millenium for degradation of azo dyes (C.I. Reactive Violet 2, and C.I. Mordant Yellow 10, hereafter: RV2 and MY10), and oxalic acid (hereafter: OX) in different reactor systems have been investigated. The influences of reactor geometry, operating mode and irradiation intensities on pollutant photocatalytic oxidation were studied. The resulting kinetic models included the effect of light absorption by dyes in water matrix, which represents a novel approach in the estimation of total photon absorption effects in photocatalytic systems.

## Experimental

### Chemicals and catalysts

The model substances were used as received from the manufacturer: oxalic acid (HPLC grade, Aldrich), C.I. Reactive Violet 2 and C.I. Mordant Yellow 10 (CIBA Limited, Switzerland). Ultrapure water was used for preparation of model solutions and analysis. Spectral data and structural representations of the dyes selected for the present work are shown in our previous publication[14]. Four different model solutions were prepared; single pollutant model solutions: RV2, MY10, oxalic acid (OX), and dye-acid mixture DAW (RV2 + MY10 + oxalic acid). Note that the respective concentration of each pollutant was 50 mg $L^{-1}$. Two different types of commercial $TiO_2$ powders: anatase-rutile P25 (Evonik) and anatase PC500 (Cristal Global – Millennium) were used for degradation of oxalic acid, MY10, RV2 and their mixture. Characteristic properties of used photocatalysts are given in our previous publication[14].

### Photocatalytic experiments and analyses

The experiments involving the utilization of UVA or UVC irradiation were performed in annular cylindrical reactors operated in batch mode (BRa and BRb), in total recirculation (TrBRa and TrBRb), or configured as CSTR. The annular cylindrical photoreactors have irradiated (working) volumes of 0.5 L and 1.5 L for reactor A and reactor B, respectively. Both reactors have sampling ports on the top, magnetic stirrer, and water jacket for temperature control (Fig. 1). The irradiation sources used were low-pressure mercury UV lamps; PenRay 90-0019-04 (365 nm) and PenRay 90-0004-07 (254 nm) all UVP-Ultra Violet Products, Cambridge, UK. UV lamps were immersed axially in a quartz tube inside the reactor. Schematics and geometric characteristics of cylindrical reactor are given in Fig. 1. Data for each photoreactor key dimensions and lamp specifications are summarized in Table 1. In the case of total recirculation mode (TrBRa and TrBRb), the photoreactor system was accompanied with a stirred tank ($V_{total}$ = 2 L). In CSTR, experimental setup consisted of feed tank ($V_{feed}$ = 6 L), reactor B, and collecting tank. All photocatalytic tests were performed in the slurry reactors. Temperature was maintained at 22.0 ± 1.5 ºC by circulating tap water through the jacket of the photoreactor. The working procedure in each photoreactor was as follows; in a typical experiment, a suspension of $TiO_2$ in selected model wastewater was prepared and transferred to the reactor (BRa and BRb) or tank (TrBRa, TrBRb, CSTR), which was fitted with a mixing unit. When working in total recircu-

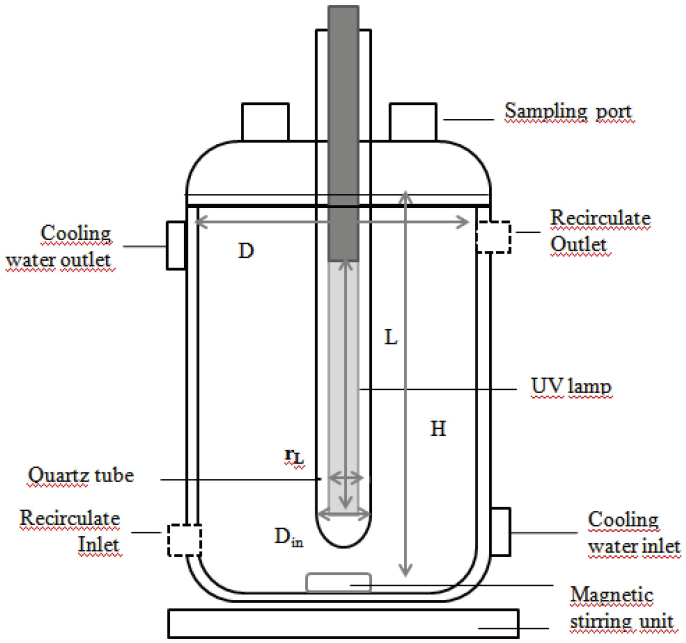


Fig. 1 – *Schematics of cylindrical photoreactors*

Table 1 – *Photoreactors specifications*

| **Photoreactor dimensions** | | |
|---|---|---|
| Photoreactor | BRa/TRBRa | BRb/TRBRb/ CSTR |
| Length, $H$ (cm) | 9.5 | 22 |
| Diameter, $D$ (cm) | 7.6 | 9 |
| Outer radius, $R$ (cm) | 3.8 | 4.5 |
| Inner radius, $\eta R$ (cm) | 0.8 | 1.2 |
| Irradiated volume, $V_r$ (dm$^3$) | 0.5 | 1.5 |
| **Lamp characteristics** | | |
| Lamp type | low-pressure mercury PenRay 90-0019-04 | low-pressure mercury PenRay 90-0004-07 |
| Primary emission output (nm) | 365 | 254 |
| Measured photon fluxes at the lamp wall, $I$ (mW cm$^{-2}$) | 10.89 | 143.3 |
| Bulb length with uniform emission, $L$ (cm) | 5.72 | 15.24 |
| Bulb radius, $r_L$ (cm) | 0.95 | 0.95 |

lation mode, the suspension was pumped to the reactor and recirculated back to the feed tank using a pulse-free peristaltic pump. In CSTR, suspension was pumped from the feed tank to reactor B and then let by free-flow to the collecting tank. The feed flow and the outflow were the same, as controlled by the height of a reaction mixture. Several cycles were performed in CSTR with different volumetric flows of reaction mixture. In the first cycle, the volumetric flow was $\nu_{0,1} = 0.37$ dm$^3$ min$^{-1}$. In other cycles (2$^{nd}$ to 7$^{th}$ cycles), volumetric flows were $\nu_{0,2} = 0.18$ dm$^3$ min$^{-1}$. The operating time for each cycle was selected according to the calculated CSTR start-up time, $t_s$. Under the assumption of isothermal reactor and first-order reaction with the rate constant $k$, the time necessary to achieve 99 % of steady-state was:

$$t_s = 4.6\frac{\tau}{1+k\tau} \qquad (2)$$

In the case when $k << 1$, Eq. (2) simplifies to $t_s = 4.6\ \tau$. Note that $\tau$ represents the CSTR space time which is equal to the hydraulic residence time ($\tau = V/\nu_0$). Having in mind $\nu_0$, $t_s$ and $\tau$ for each cycle, the total operating time for the first cycle was 17.5 minutes, while operating times for the second to seventh cycles were 35 minutes. Perfect mixing was established to obtain the homogeneous suspension in feed tank, reactor space, and collecting tank. Prior to all experiments, the initial pH of the system was adjusted using pH meter (Handylab pH/LF, Schott Instruments) at pH ≈ 4.0. The suspension was equilibrated in the dark for 30 min in the system before switching on the UV lamp. All experiments were performed in dark fume to prevent the influence of daily or ambient light. Radiometric measurements were made using radiometer (UVX, UVP) equipped with appropriate sensors.

Samples were collected at appropriate time intervals during the 120 to 240 minutes of reaction time (otherwise stated), filtered through 0.45 mm nylon filters to remove the $TiO_2$ particles, and promptly analyzed. The mineralization extents were determined based on the total organic carbon (TOC) content measurements, performed using TOC analyzer; TOC-$V_{CPN}$ 5000 A, Shimadzu. A Perkin Elmer Lambda EZ 201 UV/VIS spectrophotometer was used for monitoring decolorization at two different wavelengths, i.e., $\lambda$ = 365 nm and 550 nm that correspond to absorption maxima of MY10 and RV2, respectively. Concentrations of each dye were calculated by applying the Lambert-Beer equation to the measured absorbances at their respective $\lambda_{max}$. The concentrations of oxalic acid were determined according to the procedure described in previous publications[18,19]. To rule out the possible error due to removal of unreacted pollutant molecules absorbed to the surface of $TiO_2$ nanoparticles, additional adsorption tests in the dark were performed. The amount of pollutants filtered out with $TiO_2$ can be neglected.

## Model development

### Kinetic model

The rates of photocatalytic oxidation of organic pollutants over illuminated $TiO_2$ obeyed the Langmuir-Hinshelwood (L-H) kinetic model[9,10,20]. The L-H mechanism suggests that reaction occurs between species that are adsorbed on the surface, by assuming the adsorption and a consecutive reaction with the reactive species (•OH, $h^+$) on the catalysts surface[10]. However, the L-H model is usually simplified to an apparent first-order rate equation since the initial concentration of pollutants, $[X]_0$ does not exceed a few ppm, Eq. (3);

$$r = k\,[\mathrm{X}] \tag{3}$$

which in the case of differential reactor gives the following analytical solution:

$$[\mathrm{X}]_t = [\mathrm{X}]_0 \exp^{-kt} \tag{4}$$

A plot of $\ln([X]_t/[X]_0)$ versus time represents a straight line, the slope of which upon linear regression equals the apparent first-order rate constant $k$. The kinetic rate equations used in the present models for photocatalytic oxidation of dyes and oxalic acid were derived by considering the following assumptions[14], Eqs. (5) – (7): (i) the rates can be fitted by a L-H kinetic rate equation and their initial concentration is low, thus the L-H rate equation reduces to a first-order kinetic rate equation (n = 1), (ii) the entire reaction mechanism is based on simultaneous surface reaction with holes, $h^+$ and hydroxyl radicals, •OH. Organic molecules linked to $TiO_2$ surface via labile complexes are susceptible to •OH-attack, while the substances that bind with $TiO_2$ forming stable complexes degrade slowly via direct h+ transfer. Half and first order kinetics were chosen to define the slowest rate-determining steps for parallel reactions during the time span in the case of RV2, MY10, OX and total organic content (TOC) photocatalytic oxidation.

$$r_{\mathrm{oxalic}} = k_{1,\mathrm{obs}}\,\theta(t)\,[\text{oxalic }(t)] + \\ + k_{0.5,\,\mathrm{obs}}(1-\theta(\mathrm{t}))\,([\text{oxalic }(t)])^{0.5} \tag{5}$$

$$r_{\mathrm{dye}} = k_{1,\mathrm{obs}}\,\theta_{\mathrm{dye}}(t)\,[\text{dye }(t)] + \\ + k_{0.5,\,\mathrm{obs}}(1-\theta_{\mathrm{dye}}(t))\,([\text{dye }(t)])^{0.5} \tag{6}$$

$$r_{\mathrm{OC}} = k_{1,\,\mathrm{obs}}\,\theta_{\mathrm{OC}}(t)\,[\text{OC }(t)] + \\ + k_{0.5,\,\mathrm{obs}}(1-\theta_{\mathrm{OC}}(t))\,([\text{OC }(t)])^{0.5} \tag{7}$$

where $k_{1,\mathrm{obs}}$ and $k_{0.5,,\mathrm{obs}}$ represent the apparent rate constant for the reaction of pollutant molecules with •OH radicals and holes, respectively, [OC] denotes the molar concentration of organic content in the system (TOC/12), while $\theta(t)$ represents the surface coverage by labile complex. Note that sum of surface coverage by both complexes is 1, relating to the assumption that hydroxyl groups and oxygen occupy sites different than the pollutant[12]. Surface coverage during reaction is determined by the following expression, Eq. (8):

$$\theta_{\mathrm{X}}(t) = \mathbf{a}_{\mathrm{X}}\,[X\,(t=0)]\,(1 - \mathbf{b}_{\mathrm{X}}\,t) \tag{8}$$

where **a** and **b** represent coefficients for calculation of surface coverage at $t = 0$ and the changes in surface coverage in respect to applied irradiation. $X$ is the pollutant of concern (RV2, MY10, OX or OC).

However, the observed rate constants vary according to the set experimental conditions, and are constant for a limited range of experimental conditions. During photocatalytic experiments, the amount of applied catalyst and the corresponding surface area have a crucial effect on the $k_{\mathrm{obs}}$, and therefore, it is important to define specific reaction rate constant, $k_{\mathrm{SA}}$, Eq. (9)[21].

$$k_{\mathrm{obs}} = k_{\mathrm{SA}} \cdot \rho_{\mathrm{a}} = k_{\mathrm{SA}} \cdot a_{\mathrm{S}} \cdot \rho_{\mathrm{M}} \tag{9}$$

where, $\rho_{\mathrm{a}}$ is the concentration of $TiO_2$ surface area ($m^2\ L^{-1}$), $a_{\mathrm{S}}$ is the specific surface area measured by BET gas adsorption (56 and 340 $m^2\ g^{-1}$ for P25 and PC-500, respectively)[14], and $\rho_{\mathrm{M}}$ is the catalysts mass concentration ($TiO_2$ mass divided by working volume, $g\ L^{-1}$).

### Light absorption and scattering

The given equation can be expanded further to include the effects from light absorption and scattering on catalyst surface. For this purpose, volumetric rate of photon absorption in reaction space ($e_a$) was introduced[22]. When $e_{\mathrm{a}}$ is introduced in kinetic model, intrinsic surface reaction rate constants are obtained ($k_{\mathrm{int}}$). Volumetric rate of photon absorption depends on the irradiation type, irradiance, reactor geometry, and optical properties of the photocatalysts[22].

Local volumetric rate of photon absorption was calculated for whole reaction space in annular cylindrical reactors using the Six-flux model according to the procedure explained in previous publication[22]. Under the assumption of well-mixing, $e_a$ in the studied reactors was averaged and treated as a lumped parameter (LumpVRPA). Therefore, a central tendency of a given set of $e_{\mathrm{a}}$ values in the reaction space, $e_{\mathrm{a,\,lump}}$, has been calculated according to Eq. (10), and further used for the modeling of the photocatalytic oxidation of model wastewaters in the cylindrical reactors.

$$e_{\mathrm{a,\,lump}}(t) = \frac{1}{V_{\mathrm{R}}} \int_{V_{\mathrm{R}}} e_{\mathrm{a}}(\underline{x},t)\,\mathrm{d}V_{\mathrm{R}} \tag{10}$$

By integrating the local values of $e_a$ over the total volume of the cylindrical reactor and dividing by the same volume, the average amount of photons absorbed per unit of time and volume is obtained and introduced in kinetic models, Eqs. (11) – (13).

$$r_{oxalic} = (k_{1,int}\ \theta(t)\ [\text{oxalic}\ (t)] + \\ + k_{0.5,int}(1-\theta(t))\ ([\text{oxalic}\ (t)])^{0.5})\ a_S\ \rho_M\ e_{a,lump}(t)^{0.5} \quad (11)$$

$$r_{dye} = (k_{1,int}\ \theta_{dye}(t)\ [\text{dye}\ (t)] + \\ + k_{0.5,int}(1-\theta_{dye}(t))\ ([\text{dye}\ (t)])^{0.5})\ a_S\ \rho_M\ e_{a,lump}(t)^{0.5} \quad (12)$$

$$r_{OC} = (k_{1,int}\ \theta_{OC}(t)\ [\text{OC}\ (t)] + \\ + k_{0.5,int}(1-\theta_{OC}(t))\ ([\text{OC}\ (t)])^{0.5})\ a_S\ \rho_M\ e_{a,lump}(t)^{0.5} \quad (13)$$

Note that coefficient **b** includes the $e_a$ (**b** = **b'**$e_a$).

$$\theta_X(t) = \mathbf{a}_X\ [X][1-\mathbf{b}_X\text{'}e_a t] \quad (14)$$

Coefficients **a** and **b'** are fitted in models. Coefficient **a** was adjusted to $\theta(t = 0) \approx 0.7$ in all systems[14].

In the case of studying the wastewaters containing dyes, absorption of light (at 254 and 365 nm) by dyes should not be neglected. Decrease in the sensor readings on the wall of the reactor BRa due to the light absorption by studied dyes were calculated by the formula shown in Eq. (15);

$$\%\ I_{wall,\ sensor} = (I_{wall,\ blank} - I_{wall,\ dye})/I_{wall,\ blank} \quad (15)$$

where blank sample reading was obtained upon the irradiation of the distilled water in the annular reactor space. Obtained values were 46.4 and 79.2 %, for RV2 and MY10, respectively.

In order to obtain the correct portion of light absorbed by the photocatalyst, the following approach was established;

1. Cross-sectional area of the reactor in the radial direction was split into $N_r$ intervals.

2. Each selected interval was considered as a cell with the corresponding length, $L_r$, Eq. (16)

$$L_r = \frac{D - D_{in}}{2N_r} \quad (16)$$

3. Absorbance in the first cell and the transmitted light intensity were calculated according to the Lambert-Beer equation, Eq. (17), and using the incident photon flux entering the inner wall of the reactor, $I_0$.

$$A = \log\ (I_0/I'_0) = \varepsilon_{dye}\ [\text{dye}]\ L_r \quad (17)$$

4. The transmitted photon flux from the first cell was used as the incident photon flux entering the second cell, while the absorbance was kept constant assuming the equal concentration of dye in each cell. The procedure was repeated to the last cell.

The corrected incident photon fluxes obtained by the proposed procedure were used for the calculation of $e_a$ in the photoreactor. Molar extinction coefficients for each dye at 254 and 365 nm of irradiation were given in previous works[14,18,19].

## Reactor mass balance

While modeling the photocatalytic oxidation in the cylindrical reactors operated in batch mode, BRa and BRb, the following assumptions were made: (i) $TiO_2$ particles are evenly distributed in the reaction space, (ii) lump system can be observed in terms of the irradiation intensity and photon absorption, and (iii) limitation to the mass transfer is negligible. Regarding the general mass balance for a well-mixed, constant volume and constant temperature batch reactor is given by Eq. (18),

$$r_X = \mathrm{d}c_X/\mathrm{d}t \quad (18)$$

where $c_X$ is concentration of a pollutant in the bulk, and $r_X$ is the bulk phase rate of the same pollutant; corresponding kinetic profiles were simulated by Mathematica 9.0 (Wolfram Research) using GEAR method (backward differentiation) to find the numerical solution to the set of ordinary differential equations or the single equation.

In the case of the cylindrical reactors operated in total recirculation, TrBRa and TrBRb, the complete reaction system constitutes a closed recycling loop, between the photoreactor and the reservoir tank. The outflow concentration of the model compound from the reservoir tank becomes the ingoing concentration of the reactor, and vice versa, the mass balances of both components of the recycling loop are coupled. The reservoir tank can be modelled as a perfectly mixed continuous stirred tank. Yet, because the inlet concentration to the tank is continuously changing with time (permanent non-steady state), a time-dependent, uniform concentration exits in the tank volume as well. Photoreactor can be observed in the same manner, and the model for the continuous stirred tank reactor (CSTR) can be used. Under these assumptions, the mass balance in the reactors TrBRa and TrBRb can be written as, Eq. (19);

$$v_0 c_{X,0} - V r_X = \frac{\mathrm{d}n_X}{\mathrm{d}t} \quad (19)$$

considering a constant volumetric flow rate, $v_0$ ($dm^3\ s^{-1}$), $V/v_0$ is equal to the mean residence time, $\tau$. The equation can be finally reduced to:

$$\left(\frac{\mathrm{d}c}{\mathrm{d}t}\right)_{t_i} = \lim_{\Delta t \to 0}\left(\frac{\Delta c}{\Delta t}\right)_{t_i} = -r_{t_i} - \frac{1}{\tau}\left(c_{t_i} - c_{t_{i-1}}\right) \quad (20)$$

where $c_{t_{i-1}}$ equals the concentration at the tank outlet in time $t-1$, which equals the inlet in the photoreactor in time $t$. This model equation was solved using the finite difference method with time increments of 1 s.

A mole balance in steady-state CSTR reactor gives the following equations:

$$\text{In} - \text{Out} - \text{Degradation} = 0 \quad (21)$$

$$c_{\mathrm{X,In}} v_0 - c_{\mathrm{X,Out}} v_0 - r_{\mathrm{X}} V_{\mathrm{CSTR}} = 0 \quad (22)$$

Taking into account quasi-ideal mixing, conversion achieved in a single cycle in CSTR is written as:

$$X_{\mathrm{X}} = (-r_{\mathrm{X}})_{\mathrm{exit}} V_{\mathrm{CSTR}} / c_{\mathrm{j,In}} v_0 \quad (23)$$

where $(-r_{\mathrm{X}})_{\mathrm{exit}}$ is the rate of the reaction evaluated at the exit conditions (outlet).

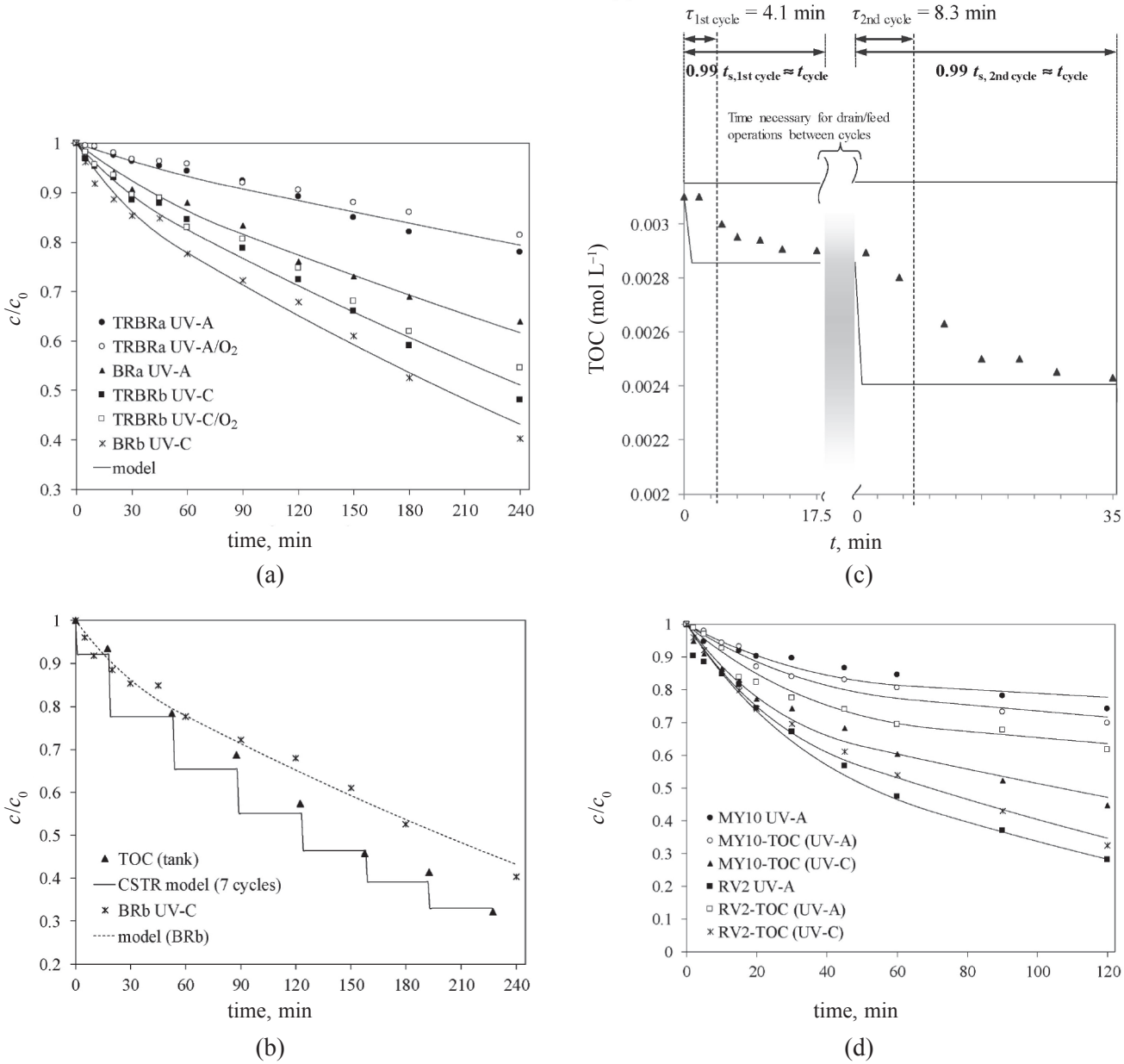


Fig. 2 – *(a) DAW mineralization kinetics (pH ≈ 4, 0.4 g dm$^{-3}$ TiO$_2$ P25) in the cylindrical reactors operated in batch and total recirculation mode using UVA and UVC irradiation, (b) Comparison between the photocatalytic experiments in BRb and CSTR operated in seven consecutive cycles (dots represent the concentration in the collecting tank after each cycle), (c) Comparison of idealized steady-state CSTR model (solid line) with the experimental TOC values as a consequence of CSTR start-up times in 1st and 2nd cycle, (d) Degradation of dyes and related mineralization in dye solutions (RV2 and MY10)*

## Results and discussion

Two groups of model pollutants: aliphatic (oxalic acid) and aromatic (azo dyes), were selected for kinetic studies of corresponding photocatalytic oxidation, due to the differences in their incident light absorption properties and the complexity of related degradation mechanisms[14,18,19]. The study of degradation and mineralization kinetics of selected pollutants by $TiO_2$ photocatalysis represents one of the main interests within this work. As elaborated in the previous section, dye (RV2 and MY10) and OX photodegradation kinetics can be modeled using the kinetic model composed from 0.5 and 1 order kinetics. The results regarding the photocatalytic oxidation of complex dye-acid wastewater (DAW) is given in Fig. 2a. The results for achieved mineralization extents in CSTR operated throughout 7 consecutive cycles are given in Fig. 2b. As may be seen, final conversion of TOC after seven cycles in reactor **b** operated as continuous stirred tank reactor is approximately 69 %, which is 1.15 times higher compared to the conversion achieved after 240 minutes of irradiation in BRb. The first cycle was performed with residence time ($\tau$) of 4.1 min, which resulted in lower conversion and the flow through the reactor was decreased in the following cycles to obtain $\tau$ = 8.3 min. Lower conversion achieved in the first cycle may be assigned to slow oxidation reactions of pollutants on the surface of irradiated photocatalyst. The model perfectly describes BR and TRBR confirming the accounted assumptions. When considering CSTR, idealized modeling approach that assumed steady-state operation throughout the cycle was adequate to predict the final concentration, since operating time for a single cycle corresponded to the CSTR start-up time ($t_s$). Deviation of measured TOC concentration in the collecting tank from the idealized model is shown in Fig. 2c. As expected for this reactor type and taking into account the experimental error (4–7 %), experimental values determined at $\tau$ correspond to 50 to 63 % of concentration at $t_s$. During selected operating times, the measured TOC approached steady-state concentration in an exponential manner. As shown in all 7 cycles, final concentration in collecting tank (TOC) corresponded to the values predicted by the model with the simple steady-state CSTR mass balance when operating time $\geq t_s$. This finding greatly simplifies the potential scale-up.

Mineralization kinetics and dye degradation kinetics are presented in Fig. 2d. Developed models followed the trend of experimental data for the concentration of particular dye during the treatment and TOC values determined in specific intervals. Determined reaction rate constants and other model coefficients are presented in Table 2. The $k_{SA,1}$, $dm^{0.5}\ s^{-1}\ W^{-0.5}$ and $k_{SA,0.5}$, $mol^{0.5}\ dm^3\ s^{-1}\ W^{-0.5}$, are intrinsic surface reaction rate constants valid for presented kinetic model and specific photocatalyst in any type of photoreactor. These constants are independent of the type of irradiation used and reactor geometries. The "intrinsic" character of the obtained

Table 2 – *Evaluation of detailed kinetic study: estimated intrinsic reaction rate constants and model coefficients*

| term | a | P25 | | | | | |
|---|---|---|---|---|---|---|---|
| | | UV-C | | | UV-A | | |
| | | $60 \cdot 10^{-6}$ $k_{SA,1}$, $dm^{0.5}\ s^{-1}\ W^{-0.5}$ | $60 \cdot 10^{-9}$ $k_{SA,0.5}$, $mol^{0.5}\ dm^3\ s^{-1}\ W^{-0.5}$ | $b' \cdot e_{a,lump}(t=0)$ | $60 \cdot 10^{-6}$ $k_{SA,1}$, $dm^{0.5}\ s^{-1}\ W^{-0.5}$ | $60 \cdot 10^{-9}$ $k_{SA,0.5}$, $mol^{0.5}\ dm^3\ s^{-1}\ W^{-0.5}$ | $b' \cdot e_{a,lump}(t=0)$ |
| OX | 950 | 6.46 | 10.91 | 0.020 | 6.54 | 12.81 | 0.010 |
| DAW (TOC) | 230 | 1.69 | 4.29 | 0.018 | 1.83 | 4.36 | 0.012 |
| RV2 | 9960 | 3.71 | 17.22 | 0.019 | 3.95 | 16.63 | 0.007 |
| MY10 | 5100 | 2.27 | 5.35 | 0.018 | 2.43 | 5.72 | 0.007 |
| | | PC-500 | | | | | |
| | | UV-C | | | UV-A | | |
| | | $60 \cdot 10^{-6}$ $k_{SA,1}$, $dm^{0.5}\ s^{-1}\ W^{-0.5}$ | $60 \cdot 10^{-9}$ $k_{SA,0.5}$, $mol^{0.5}\ dm^3\ s^{-1}\ W^{-0.5}$ | $b' \cdot e_{a,lump}(t=0)$ | $60 \cdot 10^{-6}$ $k_{SA,1}$, $dm^{0.5}\ s^{-1}\ W^{-0.5}$ | $60 \cdot 10^{-9}$ $k_{SA,0.5}$, $mol^{0.5}\ dm^3\ s^{-1}\ W^{-0.5}$ | $b' \cdot e_{a,lump}(t=0)$ |
| OX | 1100 | 2.21 | 3.19 | 0.019 | 2.16 | 2.91 | 0.011 |
| DAW (TOC) | 305 | 0.39 | 1.09 | 0.017 | 0.36 | 0.90 | 0.010 |
| RV2 | 9450 | 1.71 | 7.04 | 0.018 | 1.71 | 7.22 | 0.008 |
| MY10 | 4980 | 0.58 | 1.23 | 0.016 | 0.67 | 1.35 | 0.009 |

constants is confirmed by the similarity of constants applied for the modelling of photocatalytic degradation of studied pollutants in both BRa (TRBRa) and BRb (TRBRb) (Table 2). For instance, $k_{SA,1}$ for oxalic acid were 6.46 and 6.54 · $10^{-6}$ $dm^{0.5}$ $min^{-1}$ $W^{-0.5}$ in case of UVC and UVA irradiation, respectively, in reactors with different dimensions (Table 1).

To compare different operating modes and influence of dye on oxalic acid degradation, final conversions after 120 min of irradiation are presented in Fig. 3. Degradation of oxalic acid is highest under UVC irradiation in BRb, which corresponded to the higher photon fluxes in reaction space. The OX degradation was influenced by the presence of dyes, especially when UVA irradiation was applied. Results of OX degradation showed the negligible difference between P25 and PC-500 performance as photocatalysts under given conditions. However, the surface reaction rate constants obtained for two dissimilar photocatalysts were different (Table 2). It can be concluded that PC-500 appears equally potent as P25, but only due to its higher specific surface area (340 $m^2$ $g^{-1}$). In reality, reaction mechanisms on irradiated P25 and PC-105 surface differ slightly due to different crystalline compositions. Namely, a unique anatase/rutile content of P25 contributes to generation of higher concentration of OH radicals in comparison with pure anatase photocatalysts (as PC-500)[23].

The results regarding the mineralization in the model wastewaters containing single dyes, RV2 and MY10 pointed out the lower efficiency of UVA-assisted photocatalysis in the case of MY10 degradation and related mineralization extents. This issue was encountered previously during the photocatalytic oxidation of dyes, especially yellow dye, MY10. In the previous study, differences were observed during the application of different types of UV irradiation, i.e., photocatalytic treatment of model wastewaters resulted in various mineralization extents depending on the type of irradiation used[11,14]. Photocatalytic efficiency was influenced by the presence of dye molecules; especially by the presence of MY10, since molecules of MY10 absorb a significant portion of useful irradiation; below 380 nm. The absorption maximum for MY10 is at 365 nm, with a broad peak over 400 nm. This filtering effect of MY10 was also recognized during kinetic study; degradation of MY10 and corresponding mixtures cannot be described by the applied kinetic models in the entire time span. MY10 molecules and $TiO_2$ compete for the quantum of incident irradiation reaching catalysts surface, the intensity of which is already reduced due to absorption of a certain portion of light in the semi-transparent bulk solution. In other words, absorption of light at 365 nm by dyes cannot be neglected during accurate model development. Having in mind the maximum of absorbance at 365 nm for MY10, the portion of light absorbed by dye molecules was estimated according to the corresponding extinction coefficient, and the correction of the incident light entering each $r$ interval was taken into the account for the LVRPA calculation (as described previously).

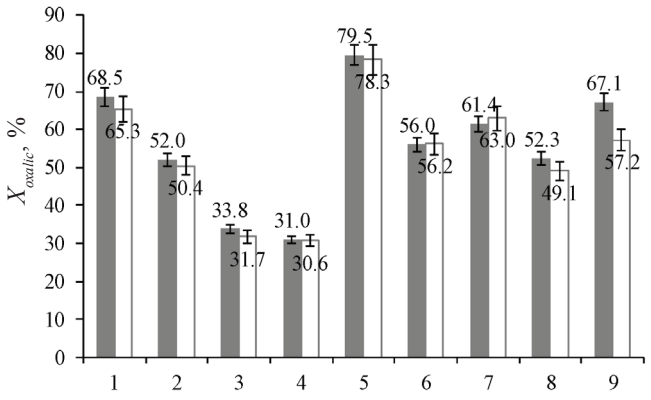


Fig. 3 – *Comparison of the average yields of oxalic acid oxidation achieved after 120 minutes treatment of UV/$TiO_2$ process in BRa (UVA, (1) – (4)), BRb (UVC, (5) – (8)) and after 4 cycles in CSTR (9). Reacting mixtures were: (1), (5) OX, (2), (6) OX + MY10, (3), (7) OX + RV2, (4)–(9) OX + MY10 + RV2 (DAW). Dark and white columns denote extents achieved using P25 and PC-500, respectively.*

In order to depict the effect of "light filtering" caused by dyes on the decrease in light intensity, forward photon fluxes were calculated for each length interval in radial direction in respect to the dye absorbance (Lambert-Beer equation), using Eq. (24).

$$I_{(r^*,z^*),forward} = \frac{\eta}{r^*}\frac{I_{(\eta R,z^*)}}{1-\gamma}\left(\frac{2\sqrt{1-\omega_{corr}^2}}{1+\sqrt{1-\omega_{corr}^2}}\right)\exp(-\tau_{app}) \quad (24)$$

Obtained radial profiles of the forward photon flux at 365 nm and 254 nm in photoreactor BRa are given in Figs. 4a and b. The negligible effect in the case of UVC irradiation was shown due to the well illuminating conditions. In particular, the incident photon fluxes observed for the UVC lamp are about 20 times greater than the ones obtained for the UVA lamp at the same nominal lamp power. Also, absorption of light at 254 nm is contributed by absorption of light due to the π-system of the aromatic ring (benzene structure) and heterocyclic triazine ring as a component of the reactive dye molecule. Concentration of dyes and the corresponding intermediates with the aromatic structure decreased during the treatment, thus allowing the increase in $e_{a,\ lump}$ with irradiation time. Having in mind the continuous degradation of dye within irradiation time, local volumetric rates of photon absorption cannot be kept constant. The continuous increase in respective values within irradiation time was taken into account for modeling purposes. Time depen-

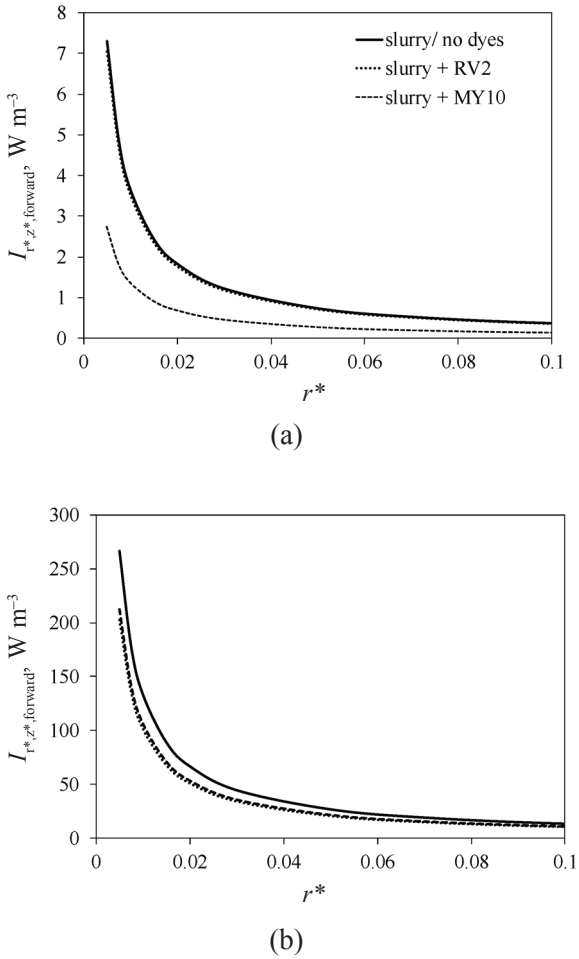


Fig. 4 – *Radial profiles of the forward photon flux in cylindrical photoreactors BRa (a) and BRb (b) with light emission maxima at 365 and 254 nm (z* = 0.5, 0.4 g $TiO_2$ P25 $L^{-1}$)*

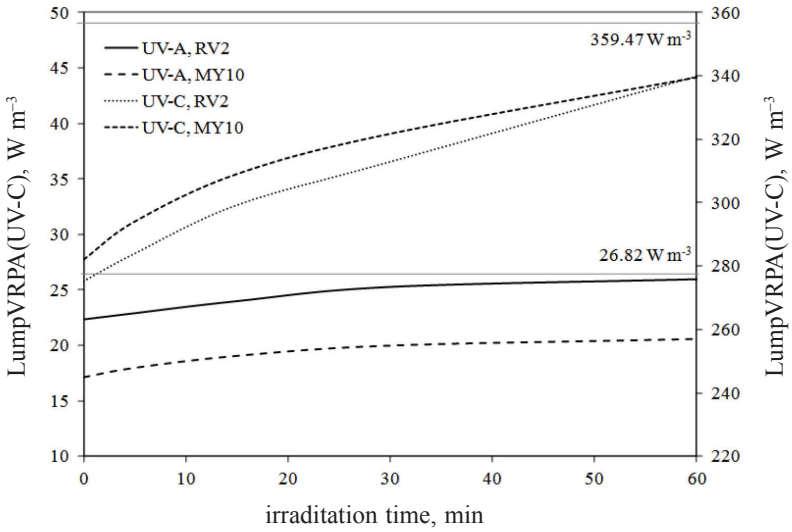


Fig. 5 – *Time dependence of the LumpVRPA in the cylindrical reactors BRa at 365 nm and BRb at 254 nm due to the change in dye and intermediates concentration during the applied process*

Table 3 – *LumpVRPA given in W m$^{-3}$ ($C_{photocatalyst}$ = 0.4 g $L^{-1}$); values at t = 0*

| reactor → reacting system ↓ | BRa/TRBRa | BRb/TRBRb/CSTR |
|---|---|---|
| P25/OX | 26.82 | 359.47 (σ + κ from Yang *et al.* (1xy)) |
| PC-500/OX | 27.60 (σ + κ estimated from extinction measurements (xy scatter.coeff)) | 450.13 |
| P25/RV2 | 22.33 | 275.25 |
| P25/MY10 | 17.09 | 282.33 |
| PC-500/RV2 | 27.25 | 438.81 |
| PC-500/MY10 | 27.33 | 442.00 |

dency of $e_{a,\,lump}$ is shown in Fig. 5. Lump values of photon absorption are summarized in Table 3.

Operation of the cylindrical reactors allowed variation between closed batch reactor (BR) and the batch reactor in recirculation (TrBR). Cylindrical reactors are more or less open, allowing the air to diffuse freely into the reaction mixture, leaving a sufficient amount of dissolved oxygen. However, to compare all the modes and reactors used, bubbling oxygen was introduced to the system at some point. As far as concerns the availability of oxygen for the photocatalytic degradation, it can be concluded that, in the case of cylindrical reactors, the concentration of dissolved oxygen originating from the air entering freely through the port on the top should be enough. In particular, while operating in batch mode, BRa or BRb, the existence of $O_2$ bubbles is undesirable in the illuminated space. Referring to the results of the UVA photolysis of oxalic acid in the TRBRa, bubbling of oxygen in the recirculation tank contributed approximately 3–5 percent to the overall oxidation yield achieved after 60 minutes of the process (data not shown). In other cases, additional oxygen caused lower degradation extents. Apart from discussion on CSTR operated in 7 cycles, it can be seen that the process performed in the BRb using the UVC irradiation yielded the highest conversion of all studied pollutants (RV2, MY10, OX) as well as the highest mineralization extents. It needs to be noted that the incident photon fluxes observed for the UVC lamp are about 20 times greater than the ones obtained for the UVA lamp at the same nominal lamp power. The lower

yields obtained for the photocatalysis in the cylindrical reactors operated in total recirculation mode, TRBRa and TRBRb, can be explained by higher total volume to reactor volume ration in the first place, and to some extent by the imperfect flow distribution, existence of backmixing, and overall non-uniform distribution of photocatalyst loading in the connecting tubes. In the cylindrical reactors, developed turbulent flow has to be achieved to have the desired degree of suspension and pseudo-uniform distribution of photocatalytic particles. In any other case, SFM cannot be implemented.

Having in mind all said, it can be concluded that the cylindrical photoreactors had a satisfying geometry for the slurry photocatalytic experiments, but only for the investigations on a laboratory scale. The dye wastewaters studied in dilution had some impact on the observed photon effect in the reaction space. It is quite easy to assume that the higher concentration of dyes with the maximum of absorbance near 365 nm would present an obstacle for UVA photocatalysis. Upon obtaining the necessary data on the radiation field characteristics in the studied reactor configurations, an adequate modeling of the $TiO_2$ photocatalytic oxidation of the studied pollutant were performed. All the results showed a good match between experimental data and model predictions. The assumption of kinetic models based on two parallel mechanisms for dyes and oxalic acid has been confirmed. All the constants presented in Table 2 are independent of the photon effects owing to the successful introduction of SFM concept and lump value of local volumetric rates of photon absorption in reaction space in the kinetic models.

## Conclusions

Detailed kinetic models incorporating two simultaneous kinetic pathways were successfully merged with mass balances for batch reactor, batch reactor with total recirculation, and continuous stirred tank reactor. The intrinsic surface reaction rates and model parameters describing adsorption during photocatalytic oxidation of pollutants were determined. The intrinsic rate constants are independent of the irradiation conditions and reactor configuration. This gives merit to the applied model, which can be used universally to describe the rates of photocatalytic degradation of organic pollutants. Moreover, the "light filtering" (i.e. photon absorption effects) caused by organic dyes were included in the model. This novel approach enables a more accurate mathematical description of photocatalytic phenomena disregarding the influence of a matrix.

*ACKNOWLEDGMENTS*

*This work is dedicated to our dear friend and colleague Prof. Dinko Vujević (1973 – 2016).*

### References

1. *Arslan Alaton*, *I.*, *Balcioglu*, *I. A.*, *Bahnemann*, *D. W.*, Advanced oxidation of a reactive dyebath effluent: comparison of $O_3$, $H_2O_2$/UV-C and $TiO_2$/UV-A processes, Water Res. **36** (2002) 1143. doi: https://doi.org/10.1016/S0043-1354(01)00335-9
2. *Pekakis, P. A., Xekoukoulotakis, N. P., Mantzavinos, D.,* Treatment of textile dyehouse wastewater by $TiO_2$ photocatalysis, Water Res. **40** (2006) 1276. doi: https://doi.org/10.1016/j.watres.2006.01.019
3. *Konstantinou*, *I. K.*, *Albanis*, *T. A.*, $TiO_2$-assisted photocatalytic degradation of azo dyes in aqueous solution: kinetic and mechanistic investigations: A review, Appl. Catal. B **49** (2004) 1. doi: https://doi.org/10.1016/j.apcatb.2003.11.010
4. *Grčić, I., Papić, S., Koprivanac, N., Kovačić, I.,* Kinetic modeling and synergy quantification in sono and photooxidative treatment of simulated dyehouse effluent, Water Res. **46** (2012) 5683. doi: https://doi.org/10.1016/j.watres.2012.07.058
5. *Kumar, P., Kumar, S., Bhardwaj, N. K.,* Advanced oxidation of ECF bleaching wastewater using $TiO_2$ photocatalysis, IJESD **3** (2012) 501. doi: https://doi.org/10.7763/IJESD.2012.V3.275
6. *Thiruvenkatachari, R., Vigneswaran, S., Moon, J. S.,* A review on UV/$TiO_2$ photocatalytic oxidation process (Journal Review), Korean J. Chem. Eng. **25** (2008) 64. doi: https://doi.org/10.1007/s11814-008-0011-8
7. *Rodrigues, A. C., Boroski, M., Sueme Shimada, N., Garcia, J. C., Nosaki, J., Hioka, N.,* Treatment of paper pulp and paper mill wastewater by coagulation–flocculation followed by heterogeneous photocatalysis, J. Photochem. Photobiol. A **194** (2008) 1. doi: https://doi.org/10.1016/j.jphotochem.2007.07.007
8. *Chong, M. N., Jin, B., Chow, C. W. K., Saint, C.,* Recent developments in photocatalytic water treatment technology: A review, Water Res. **44** (2010) 2997. doi: https://doi.org/10.1016/j.watres.2010.02.039
9. *Bahnemann, D., Hilgendorff, M., Memming, R.,* Charge carrier dynamics at $TiO_2$ particles: reactivity of free and trapped holes, J. Phys. Chem. **101** (1997) 4265. doi: https://doi.org/10.1021/jp9639915
10. *Krýsa, J., Waldner, G., Měšťánková, H., Jirkovsky, J., Grabner, G.,* Photocatalytic degradation of model organic pollutants on an immobilized particulate $TiO_2$ layer: Roles of adsorption processes and mechanistic complexity, Appl. Catal. B **64** (2006) 290. doi: https://doi.org/10.1016/j.apcatb.2005.11.007
11. *Grčić, I.,* Modelling of the photocatalytic and sonochemical process for the wastewater treatment. Ph.D. dissertation, University of Zagreb, Faculty of Chemical Engineering and Technology, Zagreb, 2011, pp 40-60.
12. *Pozzo*, *R. L.*, *Brandi*, *R. J.*, *Cassano*, *A. E.*, *Baltanás*, *M. A.*, Photocatalytic oxidation of oxalic acid in dilute aqueous solution, in a fully illuminated fluidized bed reactor, Chem. Eng. Sci. **65** (2010) 1345. doi: https://doi.org/10.1016/j.ces.2009.10.002

13. *McMurray, T. A., Byrne, J. A., Dunlop, P. S. M., Winkelman, J. G. M., Eggins, B. R., McAdams, E. T.,* Intrinsic kinetics of photocatalytic oxidation of formic and oxalic acid on immobilised $TiO_2$ films, Appl. Catal. A **262** (2004) 105. doi: https://doi.org/10.1016/j.apcata.2003.11.013
14. *Grčić, I., Vujević, D., Žižek, K., Koprivanac, N.,* Treatment of organic pollutants in water using $TiO_2$ powders: Photocatalysis vs. Sonocatalysis, Reac. Kinet. Mech. Cat. **109** (2013) 335. doi: https://doi.org/10.1007/s11144-013-0562-5
15. *Kosanić*, *M. M.*, Photocatalytic degradation of oxalic acid over $TiO_2$ power, J. Photochem. Photobiol. A **119** (1998) 119. doi: https://doi.org/10.1016/S1010-6030(98)00407-9
16. *Guettai*, *N.*, *Ait Amar*, *H.*, Photocatalytic oxidation of methyl orange in presence of titanium dioxide in aqueous suspension. Part II: Kinetics study, Desalination **185** (2005) 439. doi: https://doi.org/10.1016/j.desal.2005.04.049
17. *Kumar, J., Bansal, A.,* Photodegradation of amaranth in aqueous solution catalyzed by immobilized nanoparticles of titanium dioxide, Int. J. Environ. Sci. Technol. **9 (**2012) 479. doi: https://doi.org/10.1007/s13762-012-0064-4
18. *Grčić*, *I.*, *Vujević*, *D.*, *Koprivanac*, *N.*, Modeling the mineralization and discoloration in colored systems by (US)$Fe^{2+}$/$H_2O_2$/$S_2O_8^{2-}$ processes: A proposed degradation pathway, Chem. Eng. J. **157** (2010) 35. doi: https://doi.org/10.1016/j.cej.2009.10.042
19. *Grčić*, *I.*, *Obradović*, *M.*, *Vujević*, *D.*, *Koprivanac*, *N.*, Sono-Fenton oxidation of formic acid/formate ions in an aqueous solution: From an experimental design to the mechanistic modeling, Chem. Eng. J. **164** (2010) 196. doi: https://doi.org/10.1016/j.cej.2010.08.059
20. *Cunningham*, *J.*, *Al-Sayyed*, *G.*, *Srijaranai*, *S.*, Adsorption of model pollutants onto $TiO_2$ particles in relation to photoremediation of contaminated water, in *Helz, G., Zepp, R.* and *Crosby, D.* (Eds.), Aquatic and surface photochemistry, Lewis Publishing, CRC Press, 1994, pp 317-349.
21. *Grčić, I., Papić, S., Žižek, K., Koprivanac, N.,* Zero-valent iron (ZVI) Fenton oxidation of reactive dye wastewater under UV-C and solar irradiation, Chem. Eng. J. **195-196** (2012) 77. doi: https://doi.org/10.1016/j.cej.2012.04.093
22. *Grčić*, *I.*, *Li Puma*, *G.*, Photocatalytic degradation of water contaminants in multiple photoreactors and the evaluation of reaction kinetics constants independent of photon absorption, irradiance, reactor geometry and hydrodynamics, Environ. Sci. Technol. **47** (2013) 13702-13711. doi: https://doi.org/10.1021/es403472e
23. *Kaplan*, *R.*, *Erjavec*, *B.*, *Pintar*. *A.*, Enhanced photocatalytic activity of single-phase, nanocomposite and physically mixed $TiO_2$ polymorphs, Appl. Catal. A **489** (2015) 51. doi: https://doi.org/10.1016/j.apcata.2014.10.018